

TUNABLE MID-IR OPTICAL PARAMETRIC
OSCILLATOR USING PERIODICALLY POLED
RUBIDIUM TITANYL ARSENATE

THESIS

Frank J. Glavic

First Lieutenant, USAF

AFIT/GEO/ENP/00M-02

DEPARTMENT OF THE AIR FORCE
AIR UNIVERSITY
AIR FORCE INSTITUTE OF TECHNOLOGY

Wright-Patterson Air Force Base, Ohio

APPROVED FOR PUBLIC RELEASE; DISTRIBUTION UNLIMITED.

20010523 018

The views expressed in this thesis are those of the author and do not reflect the official policy or position of the Department of Defense or the U. S. Government.

AFIT/GEO/ENP/00M-02

TUNABLE MID-IR OPTICAL PARAMETRIC
OSCILLATOR USING PERIODICALLY POLED
RUBIDIUM TITANYL ARSENATE

THESIS

Presented to the Faculty
Graduate School of Engineering and Management
Air Force Institute of Technology
Air University
Air Education and Training Command
In Partial Fulfillment of the Requirements for the
Degree of Master of Science in Electrical Engineering

Frank J. Glavic, B.E.

First Lieutenant, USAF

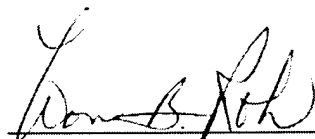
March 2000

APPROVED FOR PUBLIC RELEASE; DISTRIBUTION UNLIMITED.

TUNABLE MID-IR OPTICAL PARAMETRIC
OSCILLATOR USING PERIODICALLY POLED
RUBIDIUM TITANYL ARSENATE

Frank J. Glavic, B.E.
First Lieutenant, USAF

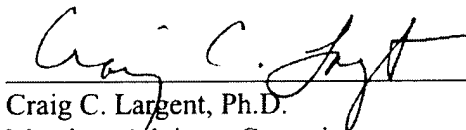
Approved:



Won B. Roh, Ph.D.
Chairman, Advisory Committee

28 Feb 2000

Date



Craig C. Largent, Ph.D.
Member, Advisory Committee

28 Feb 2000

Date



Kenneth L. Schepler, Ph.D.
Member, Advisory Committee

29 Feb 2000

Date

Acknowledgements

I would like to thank the United States Air Force and the Air Force Institute of Technology for giving me the opportunity to study a cutting-edge technological field at an outstanding educational institution. The entire faculty of AFIT has been top-notch in all aspects of instruction, advising, laboratory assistance, and personal guidance.

My sincere thanks to Dr. Won Roh for his unselfish assistance and for presenting myriad complex theories in a form I could easily understand. Thanks to Major Craig Largent for helping me work out difficult theoretical calculations when my patience had been exhausted. Also, thanks to Dr. Ken Schepler of the Air Force Research Laboratory for his guidance and for allowing me to invade his laboratory for four months.

To my wife Hyon-Chu, I am forever indebted to you for helping me through the past 18 months. You provided encouragement to help me get through many sleepless nights, and you showed infinite patience when I disappeared into study for weeks on end. Your time spent laughing and playing with our beautiful daughters, Christie and Melanie, gave me great comfort, lifted my spirits countless times, and allowed me to complete my studies knowing that our family was in good hands.

Table of Contents

	Page
Acknowledgements	iii
List of Figures.....	vi
Abstract	viii
I. Introduction	1
II. Background	5
2.1 Optical Parametric Amplification and Oscillation	5
2.2 Phase Matching Theory	7
2.3 Birefringent Phase Matching	10
2.4 Quasi-Phase Matching.....	11
2.5 Current Developments and Newer Materials	14
2.6 Electrical Poling of RTA.....	15
III. Historical Results.....	18
3.1 Monolithic OPO's	18
3.2 Elliptical Pumping.....	19
3.3 Large Aperture Crystals.....	19
3.4 Wavelength Tuning	20
IV. Experimental Setup	22
4.1 Common Equipment and Procedures	23
4.2 Conversion Efficiency Setup.....	26
4.3 Pump Depletion Setup.....	27

4.4 Spectral Linewidth Setup	28
V. Results and Analysis.....	30
5.1 Conversion Efficiency	30
5.2 Spectral Linewidth	35
5.3 Beam Quality.....	39
VI. Conclusion.....	42
Bibliography	43
Vita	48

List of Figures

	Page
Figure 1. Energy Level Diagram	2
Figure 2. Momentum Vector Diagram	2
Figure 3. The Optical Parametric Oscillator.....	3
Figure 4. Optical Parametric Amplifier.....	5
Figure 5. Singly Resonant OPO	6
Figure 6. SHG Phase-Matching Ellipsoid	11
Figure 7. QPM Crystal Schematic.....	13
Figure 8. Crystal Axes.....	15
Figure 9. RTA Poling Schematic	16
Figure 10. PPRTA Electro-Optic Monitoring	17
Figure 11. Multigrating PPLN Crystal	21
Figure 12. Photograph of the Experimental System.....	22
Figure 13. Equipment Block Diagram.....	23
Figure 14. Photograph of Optical Cavity and PPRTA Crystal.....	25
Figure 15. Pump Aligned Properly.....	26
Figure 16. Pump Misalignment.....	26
Figure 17. Conversion Efficiency Setup.....	26
Figure 18. Pump Depletion Setup	28
Figure 19. Spectral Linewidth Measurement Setup	29
Figure 20. Signal Energy vs. Pump Energy.....	32

Figure 21. PPRTA Pump Depletion at 5x Threshold.....	34
Figure 22. Pump Depletion and Signal Pulse Profile.....	34
Figure 23. Pump Depletion vs. Pump Energy	35
Figure 24. PPRTA QPM Wavelength vs. Poling Period.....	37
Figure 25. PPRTA Spectral Linewidth.....	38
Figure 26. Calculated PPRTA Signal Spectral Linewidth	38
Figure 27. PPLN Spectral Linewidth	39
Figure 28. PPRTA Signal Waist.....	40
Figure 29. PPRTA Signal at Z=720mm	40
Figure 30. PPLN Signal Waist	40
Figure 31. PPLN Signal at Z=720mm.....	40

Abstract

Tunable sources of coherent radiation are needed for a variety of military and commercial applications, including infrared countermeasures and atmospheric remote sensing. This research investigates a tunable mid-infrared coherent source using periodically-poled rubidium titanyl arsenate (PPRTA) as a quasi-phase matched (QPM) optical parametric oscillator (OPO). The advantages of PPRTA over periodically poled lithium niobate (PPLN) are presented.

Quasi-phase matching and periodic poling theory are discussed, along with some important historical results and current developments. Experimental setups for determining threshold, conversion efficiency, pump depletion, and beam quality are presented along with experimental results. The research effort is focused on characterizing PPRTA through the generation of tunable midinfrared laser radiation in the 1.4 to 4.0 micron region.

Results successfully demonstrate PPRTA conversion in the 1.5 μm range with a 173 μJ oscillation threshold and a beam quality (M^2) value of 9.0. Slope efficiency of PPRTA is shown to be 24%, compared to slope efficiency of 15% for PPLN in an identical system setup. The high slope efficiency, high pump conversion (~60%), absence of damage at pump levels in excess of 300 MW/cm^2 , and large aperture scaling possibilities suggest that PPRTA is well suited for higher power applications.

Tunable Mid-IR Optical Parametric Oscillator Using Periodically Poled Rubidium Titanyl Arsenate

I. Introduction

Since the first demonstration of an operational laser in 1960 by T. H. Maiman, (Maiman, 1960), engineers and scientists have developed numerous practical applications utilizing the high-power, coherent radiation that lasers produce. Military engineers recognized the value of directing large amounts of energy in a pencil-like beam, and have incorporated lasers into systems to defeat enemy missiles, sense remote targets, and direct munitions with pinpoint accuracy. Developments such as infrared countermeasures (IRCM) and remote environmental sensing require a laser source that can generate radiation over a broad range of wavelengths. This research effort investigates the tuning of laser radiation (which is normally output at a quasi-discrete, non-tunable wavelength) to desired wavelengths for use in development areas of great interest to the Air Force.

With a judicious choice (and orientation) of material and a suitable pump laser, one can generate radiation of desired wavelengths through nonlinear frequency conversion. Optical waves interact with materials by inducing a polarization, and if the optical field is sufficiently high, the induced polarization behaves in a nonlinear fashion. The optical waves can interact with each other and with the medium. Generating a given wavelength through nonlinear frequency conversion involves the interaction of intense laser light within a nonlinear material while satisfying two fundamental requirements:

conservation of energy and conservation of momentum. The idea of conservation of energy and conservation of momentum can be easily understood with a simple energy level diagram and a momentum vector relationship, as shown in Figure 1 and Figure 2, respectively.

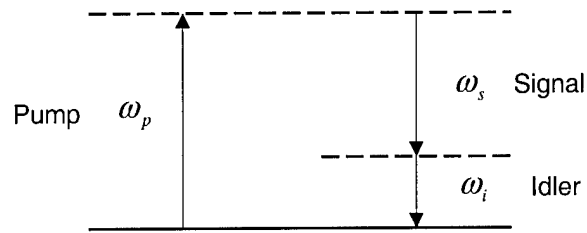


Figure 1. Energy Level Diagram

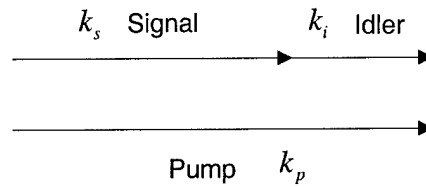


Figure 2. Momentum Vector Diagram

This experiment uses an optical parametric oscillator, schematically shown in Figure 3, to produce signal (and idler) radiation at the wavelengths of interest.

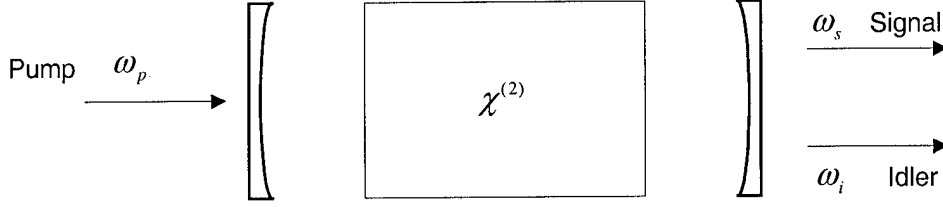


Figure 3. The Optical Parametric Oscillator

Conservation of energy is satisfied through the frequency relationship shown in Equation (1). Signal and idler radiation are generated spontaneously and amplified by the system.

$$\omega_p = \omega_s + \omega_i \quad (1)$$

Conservation of momentum (phase matching) is shown by Equation (2), which defines the wave vector mismatch, Δk . The wavelength components that satisfy the phase matching condition (*i.e.*, $\Delta k = 0$) are optimally generated in an OPO. Supporting theory is presented in Chapter 2.

$$\Delta k = k_p - k_s - k_i \quad (2)$$

Techniques to achieve phase matching have seen widespread use using birefringent materials, but the dispersion properties of the material limit the tuning range. Alternatively, quasi-phase matching, which is achieved through periodically reversing the

domain structure of a polar crystal, allows one to compensate for natural dispersion and to custom-design a crystal to meet the needs of the application (Schepler, 1997:41).

This research effort investigates a relatively new type of periodically poled material, rubidium titanyl arsenate (RTA) in a quasi-phase matched OPO. Results are compared to those using lithium niobate, which is the dominant material used in periodically poled OPO's. Performance advantages and disadvantages of RTA are offered.

Background information on optical parametric oscillation, phase matching, and periodic poling is presented in Chapter II. Previous research in this field is discussed in Chapter III. Chapter IV describes the experimental setup, and Chapter V presents experimental results. Finally, conclusions are offered in Chapter VI.

II. Background

A general understanding of optical parametric oscillation is needed before an understanding of this thesis material can be achieved. The basic properties of optical parametric oscillation will be presented below. This is followed by a presentation of phase matching theory and relevant equations. Finally, a general overview of current developments and newer materials is presented.

2.1 Optical Parametric Amplification and Oscillation

Optical parametric amplification, which was first demonstrated in 1965, involves the interaction of pump and signal photons within a nonlinear material to generate additional amounts of signal (and idler) photons (Giordmaine, *et al.*, 1965).

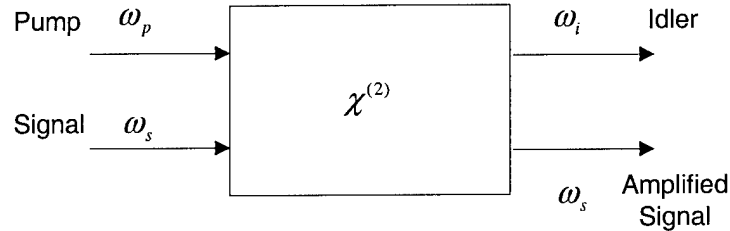


Figure 4. Optical Parametric Amplifier

The nonlinear response of the medium causes the pump and signal waves to beat and produce an idler wave at frequency ω_i ; the idler wave in turn beats with the pump

wave to produce additional signal power at ω_s . Thus, power is transferred to the signal and idler according to the Manley-Rowe relationship, Equation (3).

$$\frac{P_p}{\omega_p} = -\frac{P_s}{\omega_s} = -\frac{P_i}{\omega_i} \quad (3)$$

By placing an optical parametric amplifier inside an optical cavity, one can achieve optical parametric oscillation. When the parametric gain exceeds cavity losses, parametric fluorescence builds up to a value approaching pump intensity, and the device operates similar to a laser (Butcher, *et al.*, 1990).

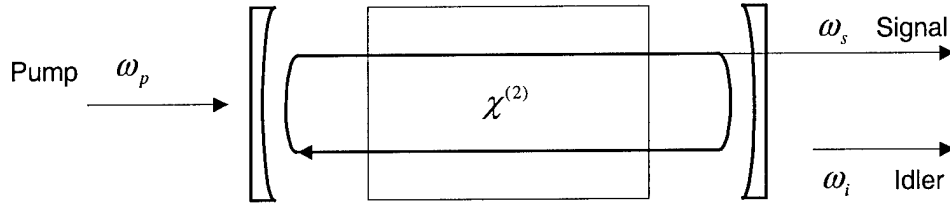


Figure 5. Singly Resonant OPO

Optical parametric oscillation, as applicable to this research effort, involves a pump beam and a PPRTA crystal which is situated in a cavity that is resonant at the mid-IR signal frequencies of interest.

2.2 Phase Matching Theory

A brief overview of phase matching considerations follows, starting with development of coupled-wave equations (Boyd, 1992:57-67).

The frequency-dependent wave equation for a dispersive medium with negligible dissipation can be derived in a straightforward manner from Maxwell's equations (Boyd, 1992:57-61), and the result is shown in Equation (4).

$$-\nabla^2 \tilde{E}_n + \frac{\epsilon^{(1)}(\omega_n)}{c^2} \cdot \frac{\partial^2 \tilde{E}_n}{\partial t^2} = \frac{-4\pi}{c^2} \cdot \frac{\partial^2 \tilde{P}_n^{NL}}{\partial t^2}, \quad (4)$$

where

\tilde{E}_n is the electric field strength at frequency component n ,

$\epsilon^{(1)}(\omega_n)$ is the frequency-dependent dielectric tensor that relates \tilde{D}_n and \tilde{E}_n ,

\tilde{P}_n^{NL} is the nonlinear polarization vector at frequency component n ,

and the tilde denotes quantities that vary rapidly in time.

For a lossless nonlinear material where the input waves are continuous, monochromatic, and at normal incidence, a solution to the wave equation for the signal frequency ω_s is given by Equation (5).

$$\tilde{E}_s(z, t) = A_s(z) e^{i(k_s z - \omega_s t)} + \text{complex_conjugate}, \quad (5)$$

where

$$k_s = \frac{n_s \omega_s}{c}, \quad (6)$$

$$\text{and } n_s = \sqrt{\epsilon^{(1)}(\omega_s)}. \quad (7)$$

The nonlinear driving term of the wave equation can be represented as

$$\tilde{P}_s(z, t) = P_s e^{-i\omega_s t} + \text{complex_conjugate}, \quad (8)$$

where the nonlinear coefficient, d , and the pump and idler waves contribute as

$$P_s = 4dA_p A_i^* e^{i(k_p - k_i)z}. \quad (9)$$

Inserting Equations (5) through (9) into the wave equation, canceling terms, and dropping the complex conjugate terms yields Equation (10).

$$\frac{d^2 A_s}{dz^2} + 2ik_s \frac{dA_s}{dz} = \frac{-16\pi d \omega_s^2}{c^2} A_p A_i^* e^{i(k_p - k_i - k_s)z} \quad (10)$$

Applying the slowly-varying-amplitude approximation to Equation (10) eliminates the first term on the left and results in the coupled-amplitude equation for the signal field shown in Equation (11). Note that the definition for wave vector mismatch, Equation (2), was introduced into the exponential. The two additional coupled-amplitude equations for the idler and pump fields can be derived in a similar fashion, and the results are shown as Equations (12) and (13).

$$\frac{dA_s}{dz} = i \frac{8\pi d \omega_s^2}{k_s c^2} A_p A_i^* e^{i\Delta k z} \quad (11)$$

$$\frac{dA_i}{dz} = i \frac{8\pi d \omega_i^2}{k_i c^2} A_p A_s^* e^{i\Delta k z} \quad (12)$$

$$\frac{dA_p}{dz} = i \frac{8\pi d \omega_p^2}{k_p c^2} A_s A_i e^{-i\Delta k z} \quad (13)$$

It can be seen from Equation (11) that for perfect phase matching ($\Delta k = 0$), the amplitude of the signal increases linearly with z ; hence, the intensity increases quadratically with z . For the general case of nonzero wave vector mismatch, the amplified signal field can be found by integrating Equation (11) across the length of the crystal, L . The result is shown in Equation (14).

$$A_s = i \frac{8\pi d \omega_s^2}{k_s c^2} A_p A_i^* \left(\frac{e^{i\Delta k L} - 1}{i\Delta k} \right) \quad (14)$$

Utilizing the relationship between intensity and amplitude of a wave given in Equation (15), and the relationship for the squared modulus given in Equation (16), the signal intensity for the field given by Equation (14) can be expressed as Equation (17).

$$I_j = \frac{n_j c}{2\pi} |A_j|^2 \quad (15)$$

$$\left| \frac{e^{i\Delta k L} - 1}{\Delta k} \right|^2 = L^2 \text{SINC}^2 \left(\frac{\Delta k L}{2} \right) \quad (16)$$

$$I_s = \frac{512\pi^5 d^2 I_p I_i}{n_p n_s n_i \lambda_s^2 c} L^2 \text{SINC}^2\left(\frac{\Delta k L}{2}\right) \quad (17)$$

Equation (17) shows the dramatic effect of phase mismatch on the output signal intensity. The phase mismatch, given by Equation (2), can be rewritten as Equation (18) for the case of perfect phase matching.

$$n_s \omega_s + n_i \omega_i = n_p \omega_p \quad (18)$$

For normal dispersion in materials, where $n_p > n_s > n_i$ for $\omega_p > \omega_s > \omega_i$, Equation (18) along with the conservation of energy relationship given by Equation (1) cannot be satisfied unless phase matching techniques are employed.

2.3 Birefringent Phase Matching

Techniques using birefringent phase matching (BPM) employ elegant combinations of polarizations and crystal angles to achieve phase matching, but have disadvantages of possible Poynting vector walk-off and limitations on the nonlinear coefficients used.

Consider second-harmonic generation and the relationship given in Equation (18); the refractive index $n(2\omega)$ must equal the refractive index $n(\omega)$ for phase matching. Figure 6 shows typical index surfaces of a uniaxial crystal with a second-harmonic phase-matching angle of θ_m . The solid circle (o-ray at ω) intersects the solid ellipse (e-ray at 2ω) at an angle of θ_m from the optic axis. The vector k^ω drawn through the intersection

identifies a direction of propagation with equal index of refraction for the two interacting waves. Thus, a pump beam oriented along the vector \mathbf{k}^ω would be phase-matched with the SHG beam, and constructively interfere throughout the length of the medium.

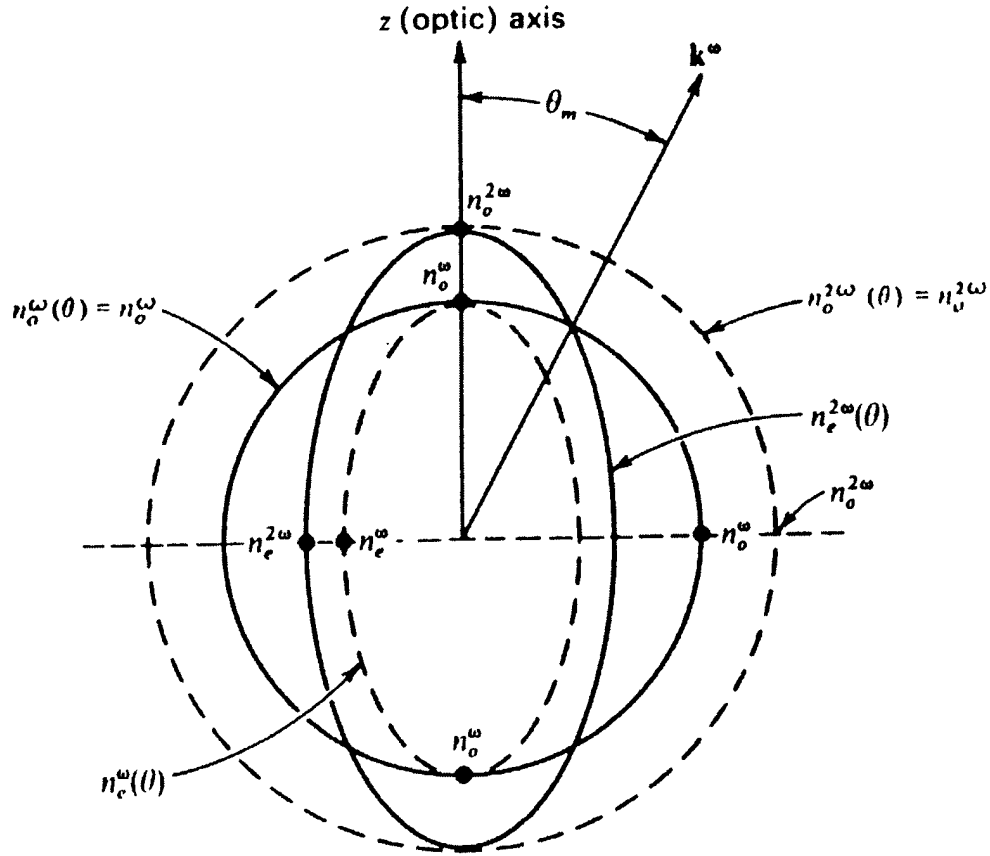


Figure 6. SHG Phase-Matching Ellipsoid
(Yariv, *et al.*, 1984)

2.4 Quasi-Phase Matching

Quasi-phase matching is a desirable alternative to BPM in which the domain of the nonlinear material is periodically reversed to compensate for phase mismatch of the interacting waves (Schepler, 1997:41). This domain reversal maintains constructive interference throughout the length of the material and can be engineered to meet the needs

of the application by constructing a poling pattern that matches that signal wavelength of interest.

With QPM, beam polarizations can be parallel, which eliminates Poynting vector walk-off and results in long interaction lengths and large nonlinear gains. The recent advances in electrical periodic poling allow intricate combinations of poling patterns that, along with temperature tuning of the crystal, allow continuous tuning of signal wavelengths over wide ranges that are limited only by the transparency of the material.

A summary of bulk QPM interaction theory is derived below (Myers, *et al.*, 1995b). The QPM effective nonlinear coefficient, d_Q , is derived from the Fourier series expansion of the single-domain nonlinear coefficient, d_{eff} . Equation (19) shows the Fourier series representation of the periodically modulated nonlinear coefficient, $d(z)$, where m represents an individual Fourier component..

$$d(z) = d_{eff} \sum_{m=-\infty}^{\infty} G_m \exp(-ik_m z) \quad (19)$$

Since the parametric process is dominated only by the phase-matched interaction, the equation simplifies to:

$$d(z) = d_{eff} G_m \exp(-ik_m z) \quad (20)$$

Using a periodic sign reversal of domains and a duty factor of D yields:

$$d(z) = d_{eff} \frac{2}{m\pi} \sin(m\pi D) \exp(-ik_m z) \quad (21)$$

Consider Figure 7, which shows the crystal axis orientation and poling period, Λ , with a 50% duty factor. For a first-order process ($m=1$), Equation (21) can be simplified to Equation (22).

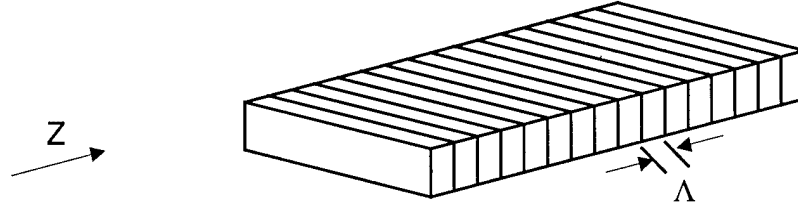


Figure 7. QPM Crystal Schematic

$$d(z) = d_{eff} \frac{2}{\pi} \exp(-i \frac{2\pi}{\Lambda} z) \quad (22)$$

Which can be rewritten as

$$d(z) = d_Q \exp(-i \frac{2\pi}{\Lambda} z) . \quad (23)$$

Equation (23), which is the final form of the periodically modulated nonlinear coefficient, can be inserted into Equations (11) through (13) to produce the coupled mode equations that describe the signal, idler, and pump waves. For quasi-phase matching, the wave vector mismatch, Δk , is now given by Equation (24).

$$\Delta k = k_p - k_s - k_i - \frac{2\pi}{\Lambda} \quad (24)$$

When $\Delta k = 0$, the grating period, Λ , is twice the coherence length, l_c , of the same interaction in single-domain material, as shown in Equation (25). This value of Λ provides a sign-change in the nonlinear polarization every coherence length, bringing the interacting waves back in phase and maintaining constructive interference.

$$\Lambda = 2l_c = \frac{2\pi}{k_p - k_s - k_i} \quad (25)$$

Equation (25) provides the grating period required for phase mismatch to equal zero; *i.e.* perfect phase matching. This demonstrates the advantage of QPM: phase matching is accomplished through engineering a suitable grating, independent of material dispersion properties.

2.5 Current Developments and Newer Materials

Periodically poled lithium niobate (LiNbO_3), the dominant material used in infrared QPM OPO's, has been successful in generating coherent radiation beyond 5.3 μm in wavelength in pulsed systems, but it is limited to small apertures and is susceptible to undesirable thermal effects and photorefractive damage (Reid *et al.*, 1997:1397).

Rubidium titanyl arsenate (RbTiOAsO_4 , or RTA), which is a crystal isomorph of potassium titanyl phosphate (KTiOPO_4 , or KTP), possesses several characteristics that make it a desirable alternative to LiNbO_3 . RTA has advantages of wider aperture crystals due to lower coercive poling field, low thermally induced lensing, and room temperature operation due to the absence of photorefractive damage (Edwards *et al.*, 1998:837;

Kennedy *et al.*, 1998:503). Disadvantages of RTA are increased crystal cost and a more elaborate poling equipment setup, as discussed in section 2.3. The advantages of RTA can be exploited to build a higher power, more practical, tunable midinfrared laser source than previously possible with PPLN.

2.6 Electrical Poling of RTA

Periodic poling of RTA presents unique challenges due to variance in the ionic conductivity of RTA from sample to sample; crystals from different growth runs may vary in conductivity by an order of magnitude. Until advances in growth techniques provide more uniform samples, poling of RTA requires a somewhat more complicated setup than that of lithium niobate. The following is a brief description of RTA poling fundamentals as described by Stolzenberger, *et al.*, 1999.

To define the poling pattern, gold (with a chromium seed layer) and aluminum electrodes are evaporated onto the (+) and (–) z-faces, respectively; reference Figure 8.

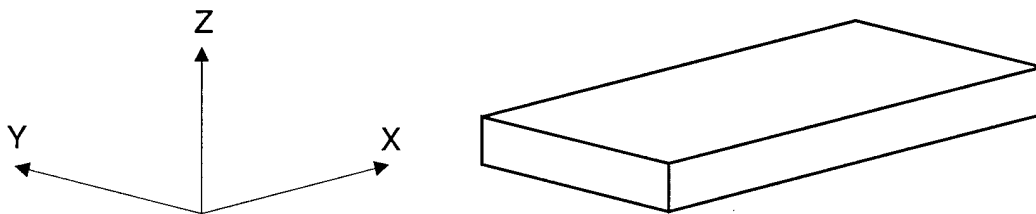


Figure 8. Crystal Axes

Standard lithography is used to define the poling pattern on the aluminum face along the x-direction; grating elements are connected together at their ends. The setup shown in Figure 9 is used to apply the high voltage coercive field.

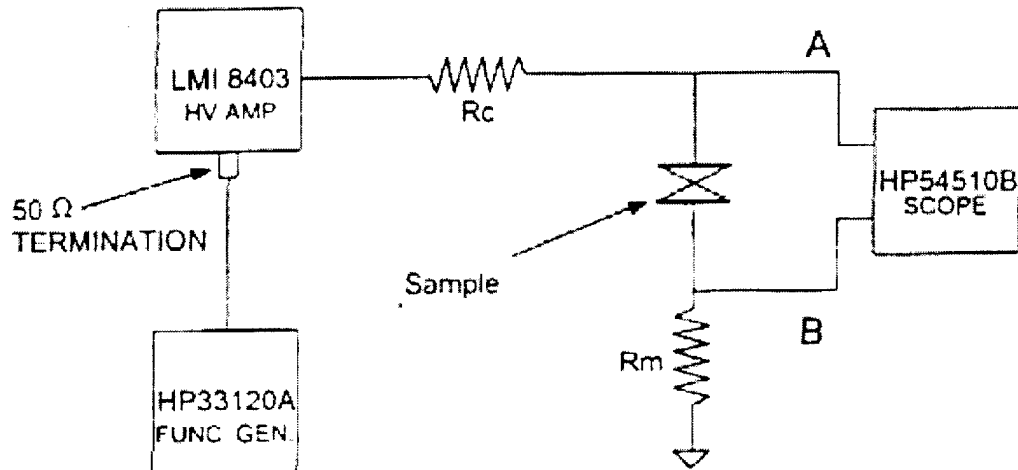


Figure 9. RTA Poling Schematic
(Stolzenberger, *et al.*, 1999)

The poling process must be carefully monitored to ensure the domain inversions are properly formed. If under-poled, the domain reversals will appear as streaks instead of the ideal rectangular form. If too many poling pulses are applied, the reversals will wash into the spaces between inversions. Both conditions lead to a diminished effective nonlinear coefficient.

In lithium niobate, uniformity of crystals allows a predefined prescription of poling current. However, current RTA samples require additional electro-optic monitoring as shown in Figure 10. The HeNe laser light is separated into ordinary and

extraordinary rays by the un-poled sample. The phase retardation between the two rays is modulated with a voltage applied to the sample electrodes and monitored by the detector. When the poling is complete, the electro-optic effect becomes zero.

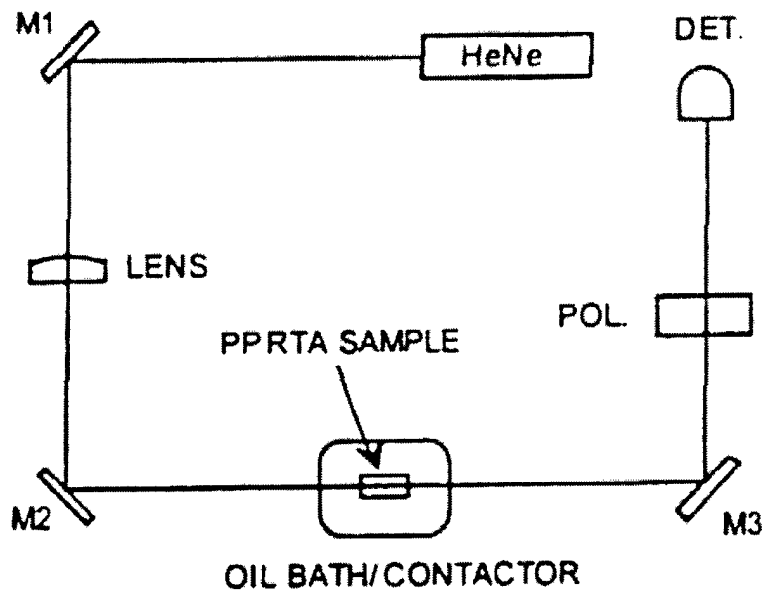


Figure 10. PPRTA Electro-Optic Monitoring
(Stolzenberger, *et al.*, 1999)

Electro-optic monitoring in combination with charge transfer monitoring provide a good indication of poling, but do not allow unique definition of the domain structure. The best method of monitoring is *in situ* monitoring of OPO output, but unique cavity and pump source configurations are required for each different PPRTA device design.

III. Historical Results

Although the theory of QPM was developed soon after demonstration of the first laser, (Armstrong, *et al.*, 1962), practical implementation proved difficult due to the micron-level grating periods required for typical nonlinear materials. The concept of patterning the domain polarity of ferroelectrics through photolithography and an applied high voltage field made bulk QPM interactions a reality (Myers, *et al.*, 1995a).

This chapter discusses advancements in the field of QPM. Monolithic OPO's utilize the crystal endfaces as the mirrors of the resonant cavity, resulting in an economical and simplistic device. Elliptical pumping better matches the pump beam to the rectangular aperture of the crystal, providing increased energy handling capacity. Large aperture devices have been developed through diffusion bonding stacks of poled crystals, but distortion problems are yet to be overcome. Novel poling patterns have been shown to provide continuous tuning over large wavelength ranges. Each of these advancements is discussed in further detail below.

3.1 Monolithic OPO's

The large nonlinear coefficients utilized in QPM coupled with the simplistic nature of monolithic OPO/OPA systems enables development of compact, stable, and easily aligned tunable sources. Input and output couplers are unnecessary, lowering cost and simplifying operator adjustments. Stability is improved by eliminating doubly resonant conditions between crystal endfaces and cavity mirrors. Monolithic PPLN devices reported in the literature provide nearly diffraction-limited performance with a

grating and temperature tuning ranges of 1.4 to 4.7 μm . Conversion efficiencies exceed 50% and threshold values are as low as 44 μJ . Monolithic devices are well suited for applications in hostile environments. (Missey, *et al.*, 1999a)

3.2 Elliptical Pumping

Coercive poling fields for lithium niobate limit the thickness of the poled crystals to the order of a millimeter; however, the width of the entrance aperture is not restricted. The limited crystal thickness generally leads to rectangular apertures at the crystal endfaces. Demonstrations using an elliptical pump beam with ellipticity of 20:1 have shown an increase in energy handling capacity of PPLN (Schepler, *et al.*, 1999). Although elliptical pump beams allow an increase in pump beam energy, the signal spectral quality and beam quality are severely degraded (Missey, 1999b). The increase in optics complexity and cost, in return for a modest increase in energy handling capability may not be justifiable for most systems.

3.3 Large Aperture Crystals

Increasing aperture size in PPLN by diffusion bonding stacks of poled crystals has shown pump energies as high as 22 mJ with 2 mJ signal outputs and slope efficiencies of 12%. Stacks of three 1 mm plates have been bonded with central regions completely fused, showing seamlessly connected domains. Scattering and beam distortion problems remain, and evidence of crystal face damage due to TIR interference hot spots exist. (Schepler, *et al.*, 1999)

The lower coercive poling field for RTA allows poling of larger aperture crystals. Recent demonstrations have shown a high degree of homogeneity in the poled domain structure for a 3 mm thick PPRTA crystal. Operating with a 2 mm pump beam diameter, a 3 mm thick sample has been pumped at 65 mJ, yielding 17 mJ output pulses with a slope efficiency of 26%. (Karlsson, *et al.*, 1999)

3.4 Wavelength Tuning

The quest for a compact, reliable, and user-friendly tunable source continues; QPM through periodic poling affords distinct advantages over other methods of phase matching, and is undoubtedly the method of choice for the heart of current tunable systems. To achieve tuning of periodically poled OPO systems, several methods are available: temperature tuning, angle tuning, and multigrating (or fan grating) crystals.

Temperature tuning is widespread with periodically poled systems, but tuning is generally restricted to relatively small wavelength ranges on the order of one micron (Myers, *et al.*, 1995a; Karlsson, *et al.*, 1999). Since heating is required to prevent photorefractive damage in PPLN, implementing an adjustable temperature controller does not significantly change system complexity; however, temperature tuning (or heating at 100 degrees C) is not desirable for many systems, such as those on an aircraft.

Angle tuning can be achieved by rotating the pump beam angle in the periodically poled crystal; however angle tuning results in restricted angular acceptance and beam walkoff, limiting the interaction length and reducing the efficiency. Demonstrations using an acousto-optic beam deflector have shown successful tuning of the non-resonant

idler from 3.1 to 3.6 μm at kilohertz repetition rates (Yang, *et al.*, 1999). In monolithic OPO's, angle tuning is achieved by simply rotating the crystal (Missey, 1999b).

The most promising systems for practical implementation of tuning rely on multigrating or fan-grating poled systems. Multigrating crystals employ a range of discrete poled periods, as shown in Figure 11, and provide tuning by means of translating the crystal from one period to another to achieve a change in wavelength. Fine-tuning between multigrating steps can be achieved through temperature tuning. Fan gratings offer a grating that changes continuously across the width of the crystal, providing a continuous change in the phase matched wavelength as the pump is translated across the face of the crystal. Fan gratings offer a distinct advantage of continuous tuning through translation of the crystal, and have shown continuous tuning from 1.375 to 4.70 μm in PPLN (Missey, 1999b).

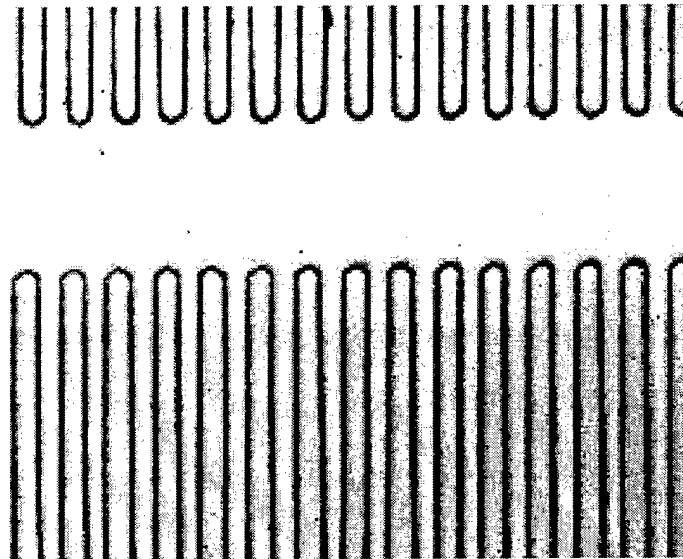


Figure 11. Multigrating PPLN Crystal

IV. Experimental Setup

This chapter describes the experimental setup and the procedures used. The chapter discusses the equipment and procedures common to all experiments, and the particular systems used for the measurement of conversion efficiency, pump depletion, and the spectral linewidth.

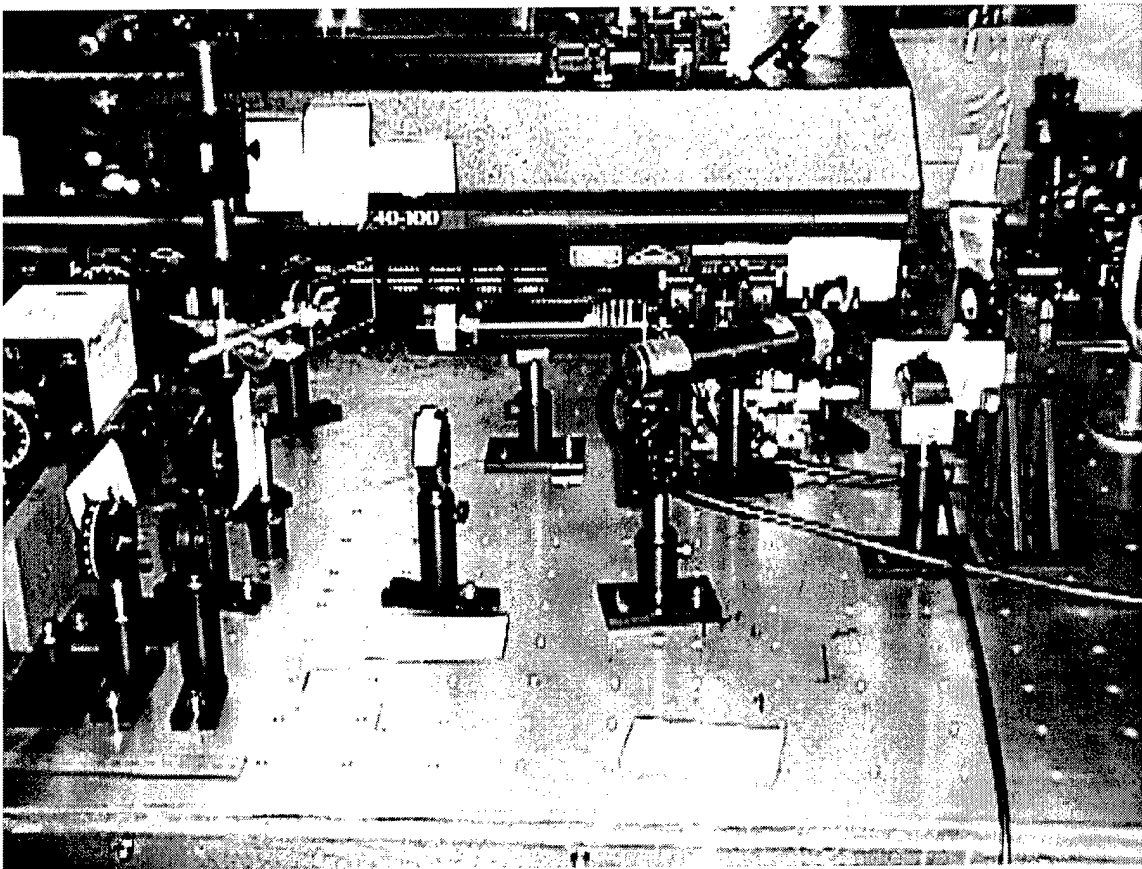


Figure 12. Photograph of the Experimental System

4.1 Common Equipment and Procedures

Figure 13 shows a schematic of the OPO and pump system, which are common to all experiments performed in this research. A Coherent Infinity Nd:YAG pulsed laser (1064 nm) operated at 30-Hz is used as the pump; the pump laser operates in single-longitudinal-mode. The pump beam is quasi-Gaussian with a top hat profile, a 5.5 mm output beam diameter, and a 0.7 milliradian divergence angle.

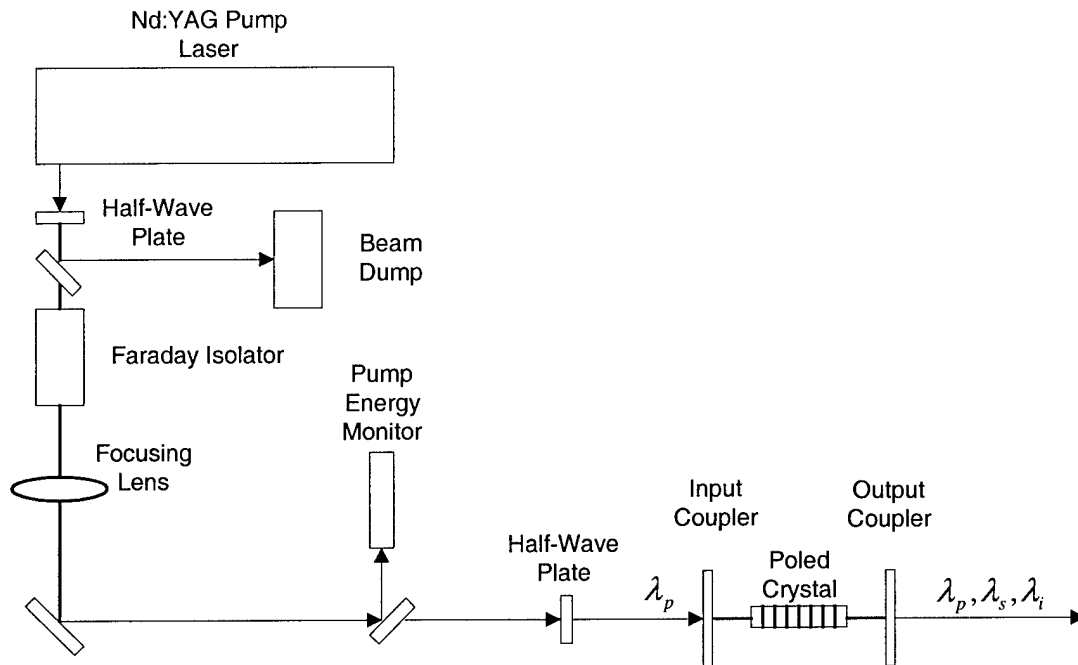


Figure 13. Equipment Block Diagram

Due to high fluctuations in pump pulse energy when operated at low output levels, the pump is operated at a higher output (200 mJ), which produces a better pulse-to-pulse

repeatability with a standard deviation of ~2%. Pump power adjustments are made via the half-wave plate and beam splitter combination located at the pump laser output. The half-wave plate and beam splitter pair operates as a variable attenuator allowing a variable portion of pump energy to be beamsplit to the beam dump. Pump energy applied to the OPO cavity is monitored through the use of a calibrated beamsplitter and a Laser Precision RJ-7620 energy ratiometer.

To maximize the nonlinear interaction volume, a plano-plano cavity is used. The cavity is single-pass for the pump, to avoid backconversion of the pump, signal, and idler waves. Cavity mirrors have signal reflectivities of 99% and 50% for the input and output couplers, respectively, and both mirrors are highly transmissive at the pump and idler wavelengths. The cavity is singly resonant at the signal wavelength of 1.45 μm , with cavity length set as small as possible, 29 mm, while still allowing the crystal to be adjusted in yaw, pitch, and roll.

The 0.5 mm thick PPRTA crystal, which was obtained from Aculight and poled by Risk at IBM, is 2.0 cm long and 1.1 cm wide with parallel and uncoated end faces. Using a laboratory microscope, the grating period is measured as 38 μm .

Characteristics of the PPRTA crystal are compared to a PPLN crystal, which is operated at the same signal wavelength using a 29 μm grating period. The available PPLN crystal has similar dimensions to the PPRTA crystal; however, the PPLN sample is slightly longer (2.5 cm). The PPLN crystal is a multigrating sample, poled at the Air Force Research Laboratory. Both crystals are operated unheated. Conversion efficiency,

pump depletion, spectral linewidth, and beam quality of the PPRTA crystal are compared to those of the PPLN crystal.

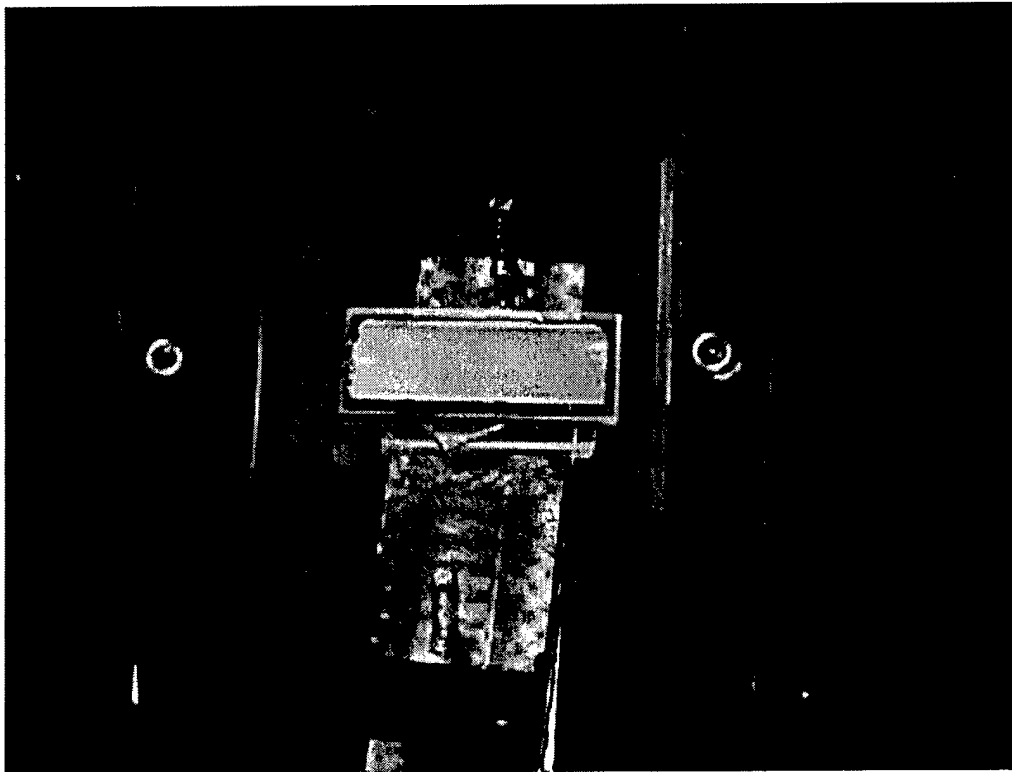


Figure 14. Photograph of Optical Cavity and PPRTA Crystal

To prevent clipping of the pump beam by the crystal, the pump beam waist is transformed by a 1000 mm focusing lens. The transformed waist is located at the center of the optical cavity with a $200\text{ }\mu\text{m}$ ($1/e^2$ intensity) radius, measured using the knife-edge technique (Suzaki, 1975).

Alignment of the cavity mirrors and crystal is performed with an IR viewer and the pinhole technique. The pump beam is directed through a pinhole in an index card,

and the mirrors and crystal are aligned such that reflections fall directly back on the pinhole. Proper alignment of the pump is verified by imaging the waist onto a Beam Code system with a Coherent Hamamatsu IR camera. Figure 15 depicts an image of the pump beam waist when properly aligned in the crystal; Figure 16 shows misalignment of the pump beam at the upper edge of the crystal.

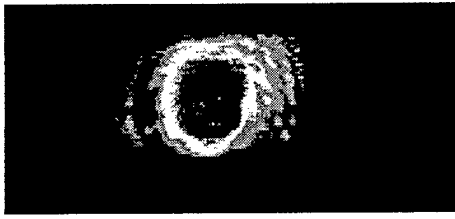


Figure 15. Pump Aligned Properly

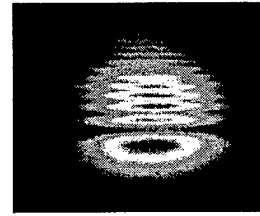


Figure 16. Pump Misalignment

4.2 Conversion Efficiency Setup

Energy conversion efficiency is determined by measuring the OPO signal power output using the setup shown in Figure 17. Residual pump energy is dumped by the 45-degree pump HR, and the signal is further isolated using the signal HR mirror.

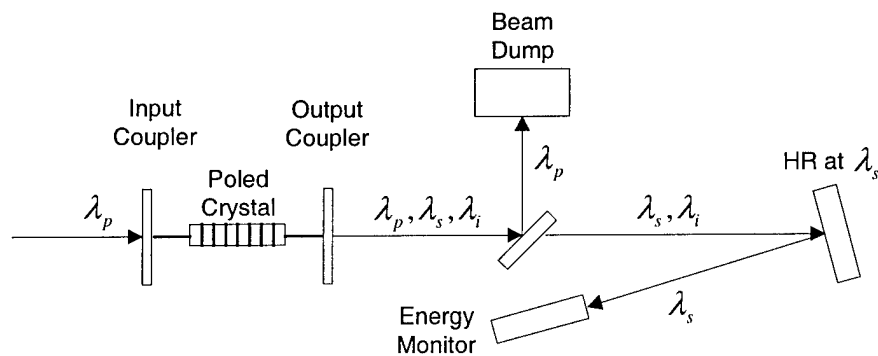


Figure 17. Conversion Efficiency Setup

Multiple iterations of cavity alignment and signal energy measurements are performed and results are presented in section 5.

4.3 Pump Depletion Setup

To characterize the effectiveness of conversion within the OPO, a pump depletion monitoring system was setup as depicted in Figure 18. By rotating the pump polarization from vertical to horizontal, the nonlinear interaction shifts from the large d_{33} coefficient of the crystal, the OPO drops below threshold, and nonlinear conversion ceases. This produces a pulse energy profile with identical cavity losses, less the depletion due to nonlinear conversion. The resulting residual pump profiles are integrated numerically in a PC-based data acquisition system, and depletion values are determined according to Equation (26).

$$\eta_{meas} = \frac{\int [P_{pump}^{undepl}(t) - P_{pump}^{depl}(t)] dt}{\int P_{pump}^{undepl}(t) dt} \quad (26)$$

After passing through the OPO, the residual pump energy is suitably attenuated by reflection off a microscope cover slide and by scattering through an index card. An InGaAs detector is situated behind the index card, and the pump pulse profile is monitored on a 1.5 GHz scope with the traces averaged over 31 pulses. With the desired depleted and undepleted traces stored in memory, the PC acquisition system gathers the information and provides a plot of the results and a numerical value for depletion.

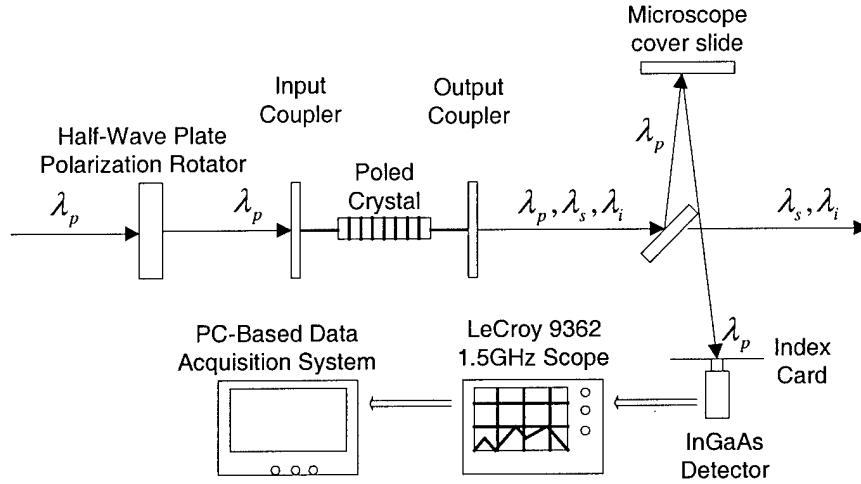


Figure 18. Pump Depletion Setup

A verification routine was performed to ensure accuracy of the detector output for the two polarizations: with the crystal removed from the cavity, the polarization was rotated from vertical to horizontal and the detector revealed identical traces for both. This provides confidence that any variation in pulse output is due to crystal effects alone.

4.4 Spectral Linewidth Setup

The output signal spectrum is characterized by focusing the OPO output into an Acton Research Spectra Pro 0.75 m monochromator, as shown in Figure 19. A 600 groove/mm grating was used along with an InGaAs detector. An automated data acquisition system was not available for characterizing the output, so the data was tabulated manually by stepping the monochromator and recording the detector output peak voltage from a 1.5 GHz scope.

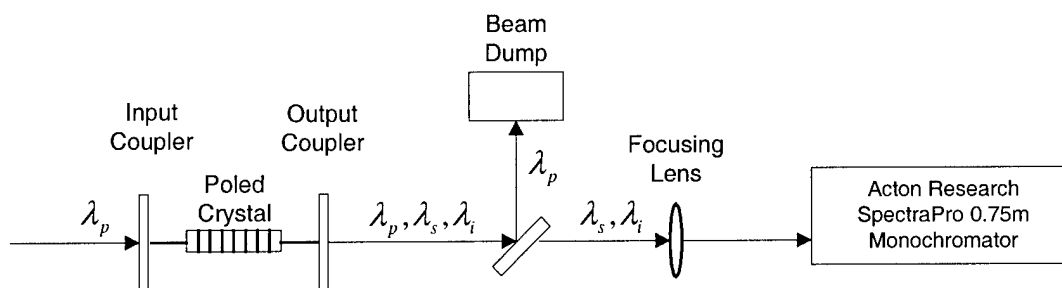


Figure 19. Spectral Linewidth Measurement Setup

V. Results and Analysis

This chapter presents the results for the various experiments described in Chapter IV. Conversion efficiency results compare PPRTA slope efficiency and threshold to those of PPLN. Output signal spectral linewidth plots are presented, followed by beam quality measurements with associated images.

5.1 Conversion Efficiency

In this section, signal energy, oscillation threshold, overall efficiency, and slope efficiency are analyzed as a function of pump energy. Figure 20 shows the signal power as a function of pump power for the PPRTA and PPLN crystals used. Error bars show \pm one standard deviation and the traces are fit to the data points. To prevent crystal damage, a maximum of 700 μJ pump energy is applied, which corresponds to a pump power density of 186 MW/cm^2 .

The measured oscillation threshold of 105 μJ for the PPLN crystal is notably lower than the 173 μJ value for PPRTA. Although this is expected due to the larger d_{33} coefficient for PPLN, the results are further biased by the fact that the available PPLN crystal has anti-reflection coated end faces while the PPRTA crystal does not. A regression fit to the PPRTA data points shows a threshold of 121 μJ , which is slightly lower than the calculated value of 140 μJ , determined from Equation (27) (Myers, *et al.*, 1995b).

$$J_T = \frac{1}{Tp} * \frac{n_p n_s n_i \epsilon_o c^3}{2\omega_s \omega_i d_Q^2} * \frac{2.25}{L^2} * \frac{w_p^2 + w_s^2}{w_p^2} * \frac{\tau}{(1 + \gamma)^2} * \cosh^{-1} \left(\frac{30L_{cav}}{2\pi c} + a_d - \ln \sqrt{Rs} \right), \quad (27)$$

where

J_T is threshold pump fluence,

Tp is the pump transmission through the input coupler and crystal face,

n_p, n_s, n_i are the refractive indices for pump, signal, and idler,

d_Q is the QPM effective nonlinear coefficient,

L is the crystal length,

w_p, w_s are the pump and signal $1/e^2$ waist sizes,

τ is the pump pulse FWHM,

γ is the ratio of backward to forward pump field amplitudes,

L_{cav} is the cavity optical length,

a_d is the signal single-pass power loss,

and Rs is the output coupler reflectivity at the signal wavelength.

Drastic changes in threshold and output signal power are observed for even minor adjustments in crystal orientation. To obtain repeatable measurements for the threshold value, the crystal is aligned at a higher pump level while monitoring signal power output. When the signal power measured is at maximum, the pump is then reduced until conversion ceases. This produced threshold results with a standard deviation of 23%.

The large deviation is attributed to etalon effects between crystal end faces and cavity mirrors. Developments with Brewster-cut or slightly wedged endfaces should reduce this problem in future experiments.

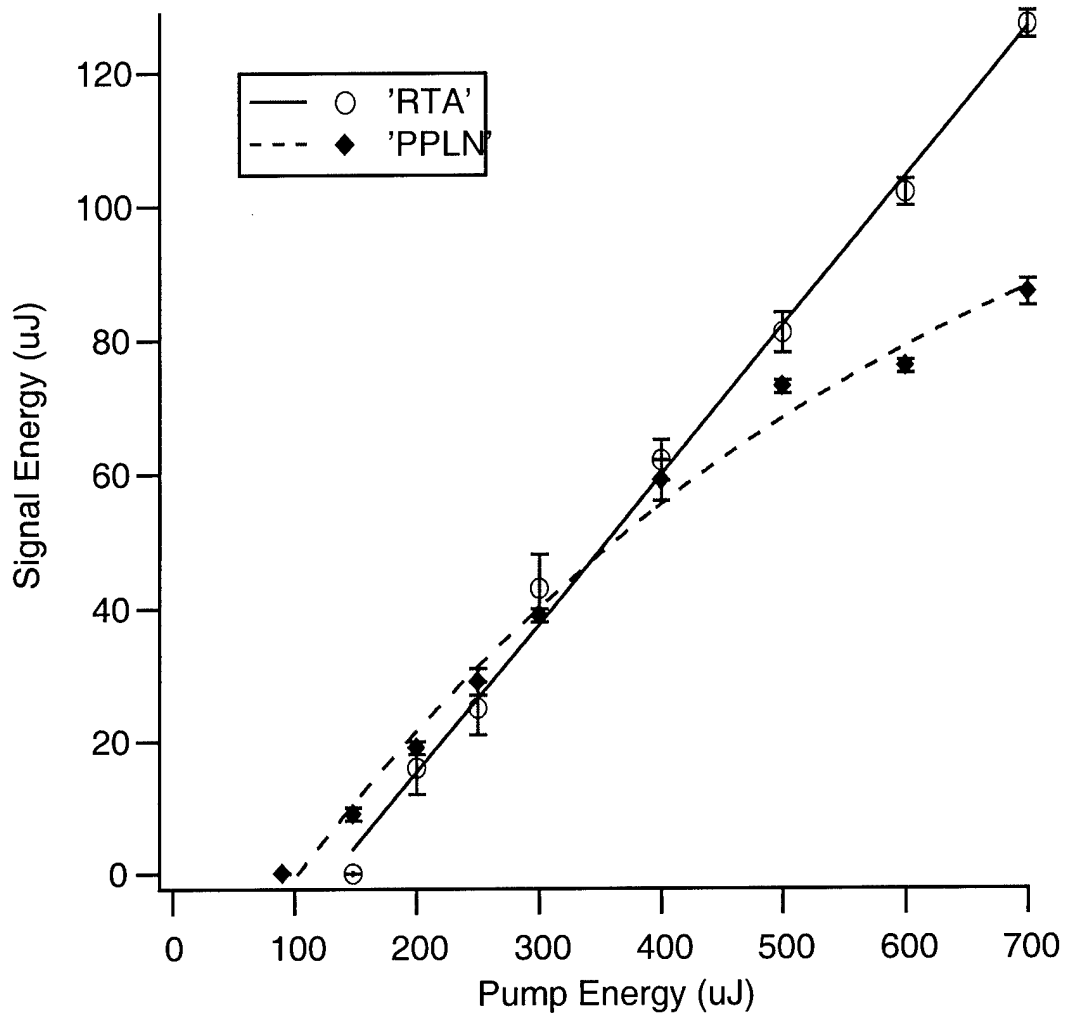


Figure 20. Signal Energy vs. Pump Energy

PPLN has the advantage of a significantly lower threshold, but PPRTA exhibits slope efficiency almost twice that of PPLN; data points along with standard deviation

bars are shown in Figure 20. At five-times threshold, overall efficiency of the PPRTA sample is 18% with a slope efficiency of 24%; these values are in excellent agreement with the calculated values for overall and slope efficiency of 19% and 25%, respectively. The PPLN exhibited overall efficiency of 12% and slope efficiency of 15% at identical pump energy. Based on power measurements, the OPO photon conversion efficiency for PPRTA at 5x threshold is 29%.

A representative plot of 51% pump depletion at five-times threshold is shown in Figure 21. The expected value for pump depletion of 35%, calculated from Equation (28), varies considerably from the measured result.

$$\%Depletion = \frac{Energy_{signal} + Energy_{idler}}{Energy_{pump} - Energy_{losses}} * 100 \quad (28)$$

Error may be attributed to anomalies with detector response and the window of data points used for the numerical integration of the experimental pulse profiles. Problems were noted during several depletion measurements where the depleted pump initial peak exceeded the undepleted pump peak, indicating a detector response problem or a computer data acquisition problem.

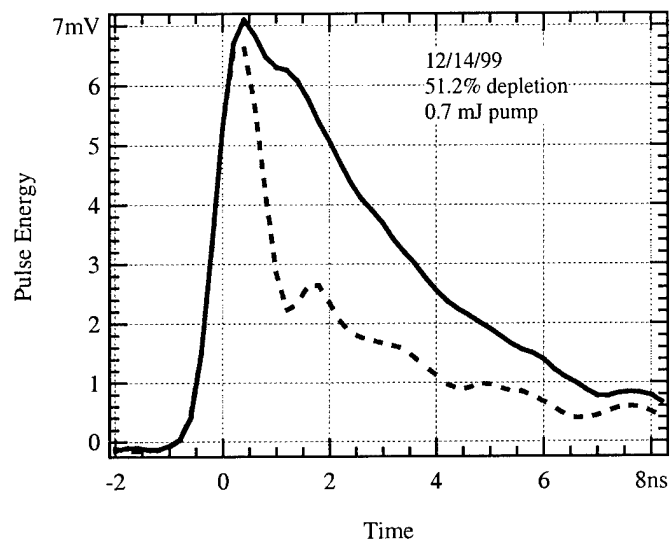


Figure 21. PPRTA Pump Depletion at 5x Threshold

The depleted trace displays an initial peak while the signal builds up to oscillation threshold, after a ~ 0.5 ns delay. This results in a slightly narrower signal pulse (~ 2.5 ns) as compared to the pump pulse (~ 3.5 ns). The signal pulse (dot-dash) along with undepleted pump (solid) and depleted pump (dash) pulses are shown in Figure 22.

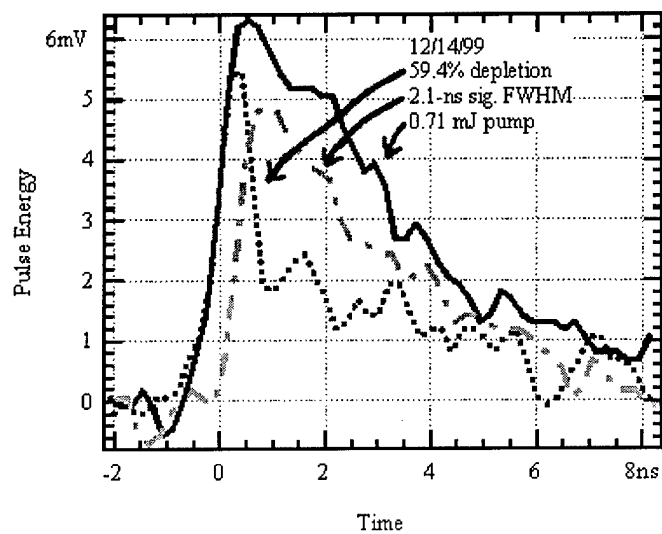


Figure 22. Pump Depletion and Signal Pulse Profile

Experimental pump depletion values as a function of pump power are plotted in Figure 23. PPRTA and PPLN exhibit nearly identical depletion values, peaking at approximately 55%, offset slightly by the different oscillation thresholds.

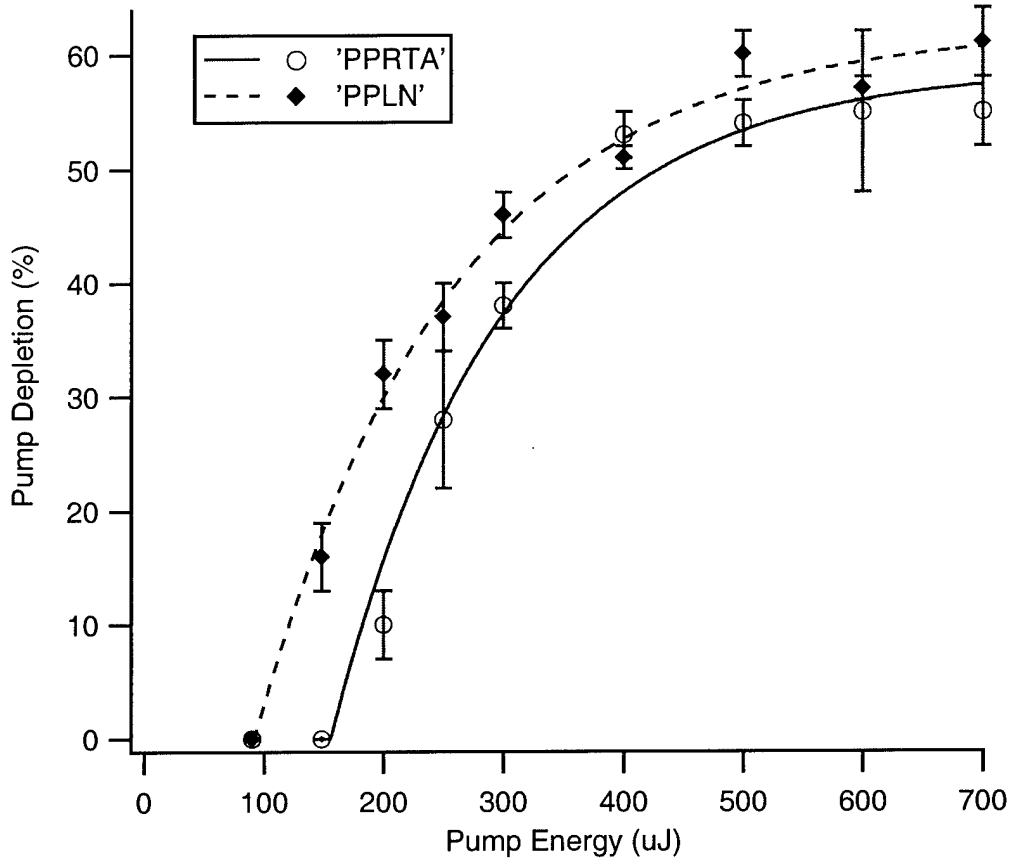


Figure 23. Pump Depletion vs. Pump Energy

5.2 Spectral Linewidth

Calculated signal and idler wavelength as a function of grating period for PPRTA are shown in Figure 24. Values are plotted numerically using the grating period

calculation, Equation (29), and the interacting wavelength relationship, Equation (31), which is easily derived from Equation (1).

$$\Lambda = \frac{2\pi}{k_p - k_s - k_i} \quad (29)$$

where

$$k_\lambda = \frac{2\pi n_z(\lambda)}{\lambda} \quad (30)$$

and

$$\frac{1}{\lambda_s} = \frac{1}{\lambda_p} - \frac{1}{\lambda_i} \quad (31)$$

Pump polarization is along the crystal z-axis. The Sellmeier equation for n_z , the index of refraction for polarization along the z-axis, is shown in Equation (32) (Fenimore, *et al.*, 1996).

$$n_z(\lambda) = \left[2.18962 + \frac{1.30103}{1 - \left(\frac{0.22809}{\lambda} \right)^2} - 0.01390\lambda^2 \right]^{\frac{1}{2}} \quad (32)$$

For the crystal grating of 38 μm , a signal wavelength of 1.424 μm is expected.

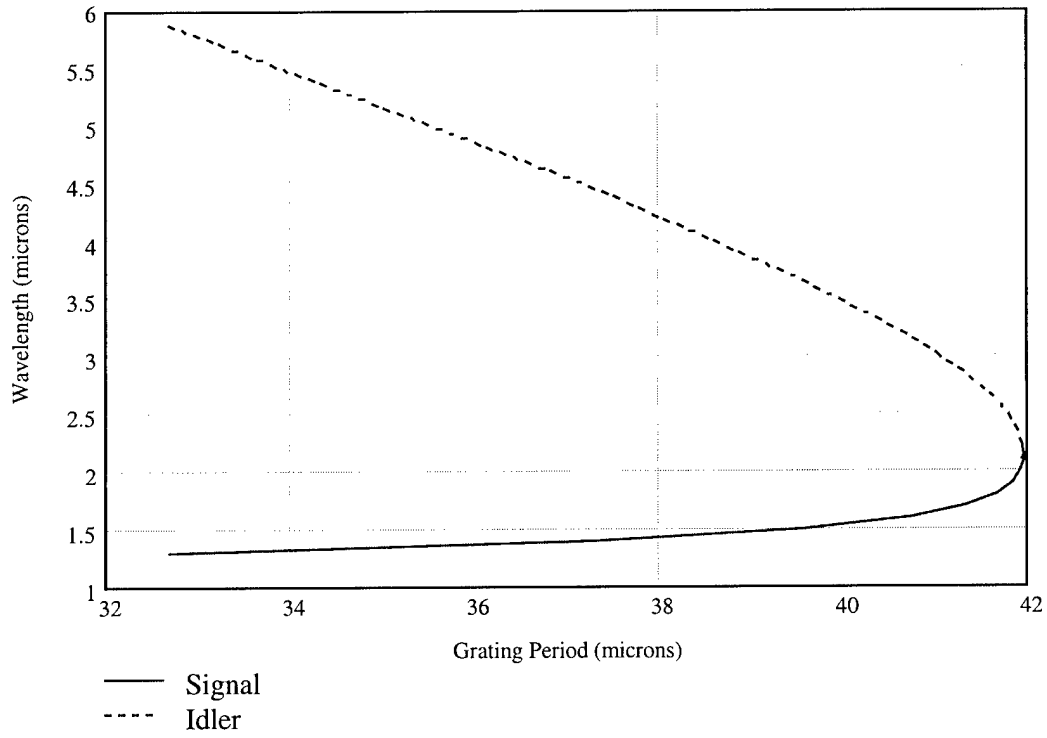


Figure 24. PPRTA QPM Wavelength vs. Poling Period

Experimental measurements of signal wavelength vary slightly from the calculated value of 1.424 μm , but the measurements are highly noisy as shown by the standard deviation error bars in Figure 25. The linewidth of 0.75 nm agrees well the calculated spectrum shown in Figure 26, which was generated using the relationship for single-pass parametric power amplification (G) as a function of phase mismatch (Δk) and crystal length (L) given by Equation (33) (Boyd, 1992:66).

$$G \propto \text{SINC}^2\left(\frac{\Delta k * L}{2}\right) \quad (33)$$

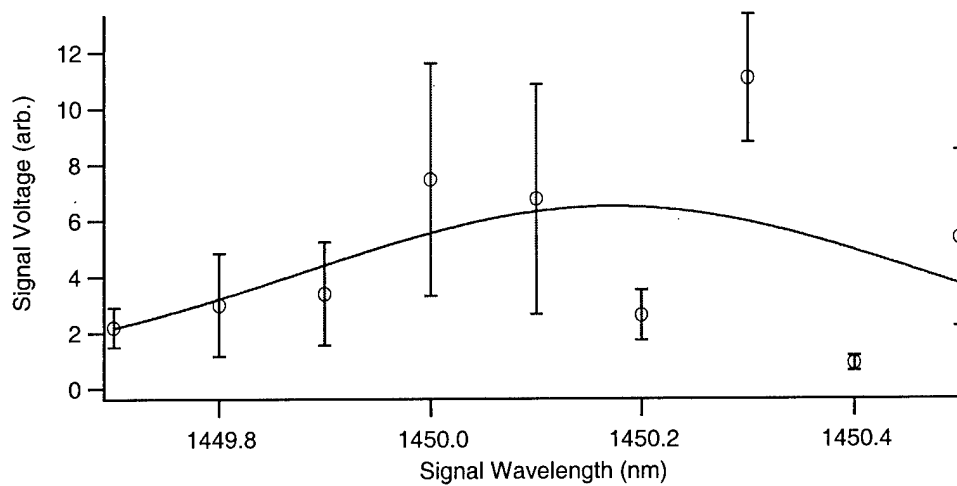


Figure 25. PPRTA Spectral Linewidth

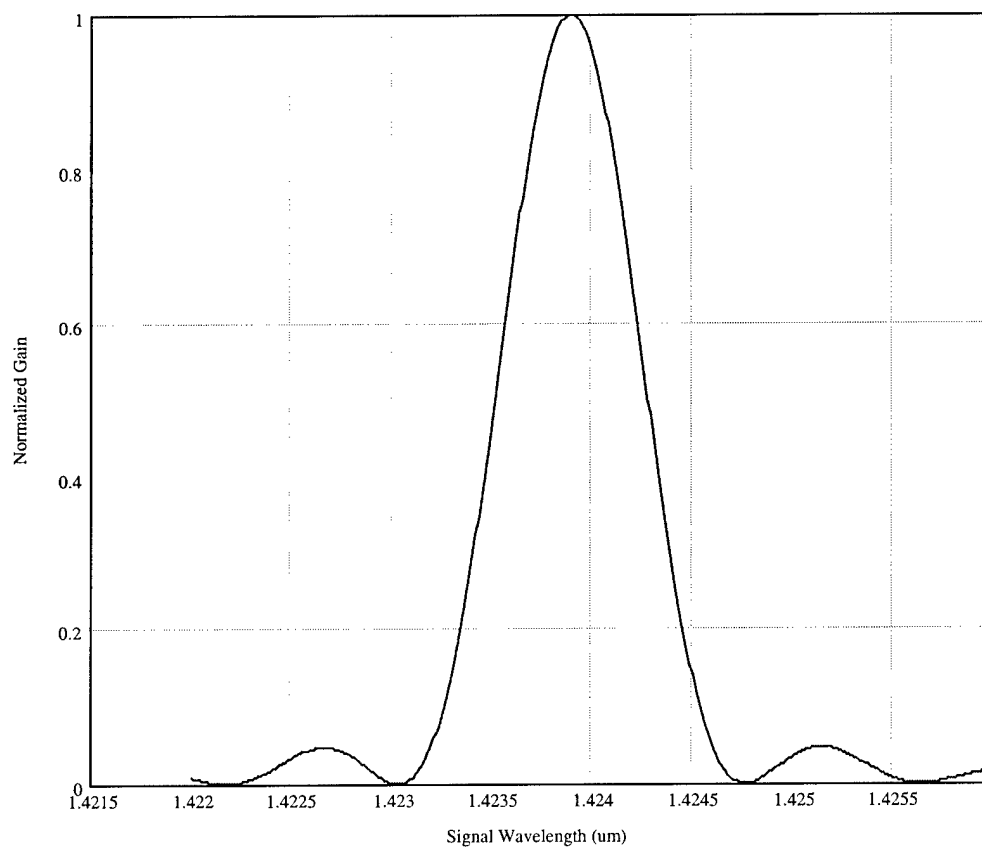


Figure 26. Calculated PPRTA Signal Spectral Linewidth

The ~26 nm peak offset may be attributed to crystal temperature difference from that used in the Sellmeier equations (Fenimore, *et al.*, 1996). Noise level variations are likely due to etalon effects in the uncoated crystal. PPLN exhibited a much broader spectrum with less noise, as shown in Figure 27.

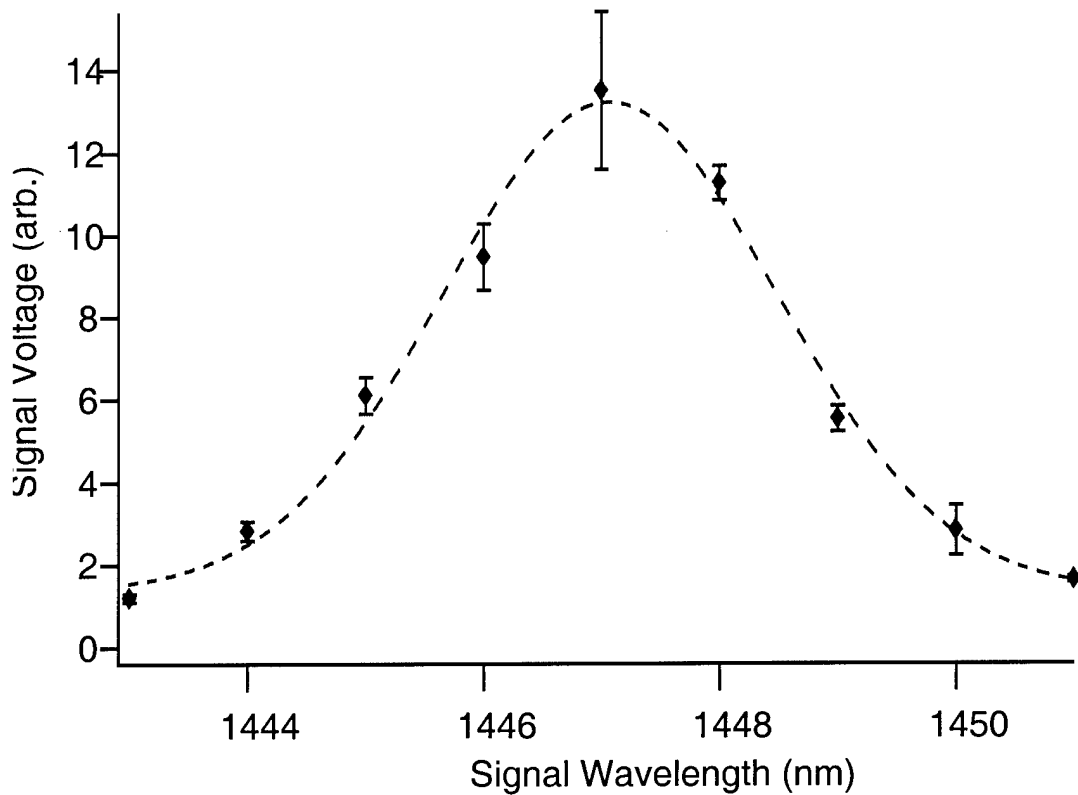


Figure 27. PPLN Spectral Linewidth

5.3 Beam Quality

Beam quality measurements were calculated using spot size measurements determined with a sliding razor blade setup. Using the 200 μm waist size and the mean

value of measured spot size, Equation (34) revealed M^2 (or, times-diffraction-limited) values of 9.0 and 11.8 for PPRTA and PPLN, respectively (Ruff, *et al.*, 1992).

$$M^2 = \frac{4\pi w_o w_z}{z\lambda} \quad (34)$$

Images of the signal beam waist and far-field spot are shown in Figure 28 through Figure 31. The beam waist was imaged from the center of the crystal to the IR camera using an optical relay, while the far-field spot was captured directly by the IR camera. The PPRTA signal displays a nice quasi-Gaussian profile, while the PPLN signal is notably distorted.

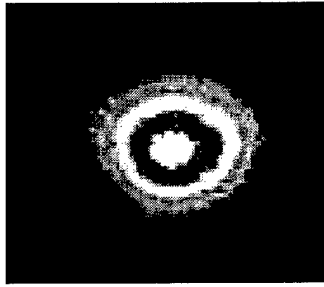


Figure 28. PPRTA Signal Waist

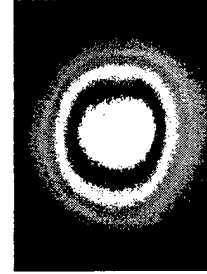


Figure 29. PPRTA Signal at Z=720mm

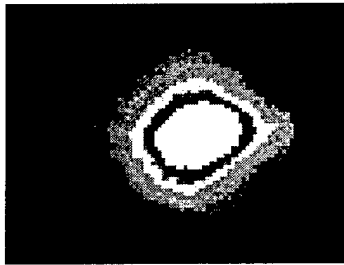


Figure 30. PPLN Signal Waist

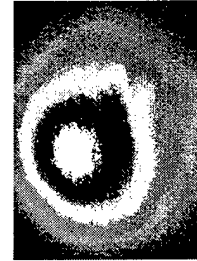


Figure 31. PPLN Signal at Z=720mm

The aberration in the PPLN beam image may be attributed to the narrow width of the 29 μm grating with respect to the pump waist size. Although Figure 30 shows only minor distortion at the signal waist, the slightly longer length of the PPLN crystal may allow the beam diameter to exceed the grating width, resulting the distortion shown in Figure 31.

VI. Conclusion

This research demonstrated the use of a quasi-phase matched PPRTA OPO as a tunable source of coherent radiation that can be applied to variety of military and commercial applications, including infrared countermeasures and atmospheric monitoring. Although the device tested had a single grating period, theory has been developed showing the possibility of multiple grating and fan grating poling patterns that can provide a continuous range of output wavelengths.

Experiments successfully demonstrated PPRTA conversion in the 1.5 μm range with a 173 μJ oscillation threshold and a beam quality (M^2) value of 9.0. Slope efficiency of 24% for PPRTA was shown to be approximately double that of PPLN in an identical system setup. High slope efficiency, high pump conversion ($\sim 60\%$), absence of damage at pump levels in excess of 300 MW/cm^2 , and large aperture scaling possibilities suggest that PPRTA is well suited for higher power applications.

Bibliography

- Arisholm, Gunnar and Knut Stenersen. "Optical parametric oscillator with non-ideal mirrors and single- and multi-mode pump beams," Optics Express, 4: 183-192 (March 1999).
- Armstrong, J. A., N. Bloembergen, J. Ducuing, and P. S. Pershan. "Interactions between light waves in a nonlinear dielectric," Physical Review, 127: 1918-1925 (September 1962).
- Baldwin, George C. An Introduction to Nonlinear Optics. New York: Plenum Press, 1969.
- Bortz, Michael L. Quasi-Phasematched Optical Frequency Conversion in Lithium Niobate Waveguides. Ph.D. dissertation. Stanford University, Stanford CA, 1994 (G.L. No. 5259).
- Bosenberg, Walter R., Alexander Drobshoff, Jason I. Alexander, Lawrence E. Myers, and Robert L. Byer. "Continuous-wave singly resonant optical parametric oscillator based on periodically poled LiNbO₃," Optics Letters, 21: 713-715 (May 1996a).
- , Alexander Drobshoff, Jason I. Alexander, Lawrence E. Myers, and Robert L. Byer. "93% pump depletion, 3.5-W continuous-wave, singly resonant optical parametric oscillator," Optics Letters, 21: 1336-1338 (September 1996b).
- Boyd, Robert W. Nonlinear Optics. Boston: Academic Press, 1992.
- Budni, P. A., M. G. Knights, E. P. Chicklis, and K. L. Schepler. "Kilohertz AgGaSe₂ optical parametric oscillator pumped at 2 μ m," Optics Letters, 18: 1068-1070 (July 1993).
- Butcher, Paul N. and David Cotter. The Elements of Nonlinear Optics. Cambridge: Cambridge University Press, 1990.
- Dereniak, E. L. and G. D. Boreman. Infrared Detectors and Systems. New York: John Wiley & Sons, 1996.
- Edwards, T. J., G. A. Turnbull, M. H. Dunn, M. Ebrahimzadeh, Hakan Karlsson, Gunnar Arvidsson, and Fredrik Laurell. "Continuous-wave singly resonant optical parametric oscillator based on periodically poled RbTiOAsO₄," Optics Letters, 23: 837-839 (June 1998).

- Englander, A., R. Lavi, and S. Jackel. "Tunable intracavity RbTiOAsO₄ OPO in the mid-IR," SPIE, 3110: 285-286 (September 1997).
- Fenimore, D. L., K. L. Schepler, D. Zelmon, S. Kuck, U. B. Ramabadran, P. Von Richter, and D. Small. "Rubidium titanyl arsenate difference frequency generation and validation of new Sellmeier coefficients," J. Opt. Soc. Am. B, 13: 1935-1940 (September 1996).
- Fernelius, Nils C., F. K. Hopkins, and M. C. Ohmer. "Nonlinear optical crystal development for laser wavelength shifting at AFRL Materials Directorate," SPIE, 3793: 2-8 (July 1999).
- Giordmaine, J. A. and Robert C. Miller. "Tunable coherent parametric oscillation in LiNbO₃ at optical frequencies," Physical Review Letters, 14: 973-976 (June 1965).
- Goodman, Joseph W. Introduction to Fourier Optics (Second Edition). New York: McGraw Hill, 1996.
- Grayson, T. P., L. E. Myers, M. D. Nelson, and Vince Dominic. "Synchronous pumping of a periodically poled LiNbO₃ optical parametric oscillator," OSA TOPS on Advanced Solid-State Lasers, 1: 46-50 (1996).
- Hecht, Eugene. Optics (Third Edition). Massachusetts: Addison-Wesley, 1998.
- Karlsson, H., M. Olson, G. Arvidsson, F. Laurell, U. Bader, A. Borsutzky, R. Wallenstein, S. Wickstrom, and M. Gustafsson. "Nanosecond optical parametric oscillator based on large-aperture periodically poled RbTiOAsO₄," Optics Letters, 24: 330-332 (March 1999).
- Kennedy, G. T., D. T. Reid, A. Miller, M. Ebrahimzadeh, H. Karlsson, G. Arvidsson, and F. Laurell. "Near- to mid-infrared picosecond optical parametric oscillator based on periodically poled RbTiOAsO₄," Optics Letters, 23: 503-505 (April 1998).
- Klein, M. E., D. H. Lee, J. P. Meyn, K. J. Boller, and R. Wallenstein. "Singly resonant continuous-wave optical parametric oscillator pumped by a diode laser," Optics Letters, 24: 1142-1144 (August 1999).
- Maiman, T. H. "Optical and microwave-optical experiments in ruby," Physical Review Letters, 4: 564-566 (June 1960).
- McKelvey, John P. Solid State Physics. Malabar FL: Krieger Publishing, 1993.

- Missey, Mark J., Vince Dominic, Lawrence E. Myers, and Robert C. Eckardt.
 "Diffusion-bonded stacks of periodically poled lithium niobate," Optics Letters,
 23: 664-666 (May 1998).
- , Vince Dominic, Peter E. Powers, and Kenneth L. Schepler. "Periodically poled
 lithium niobate monolithic nanosecond optical parametric oscillators and
 generators," Optics Letters, 24: 1227-1229 (September 1999a).
- , Monolithic PPLN Devices. Ph.D. dissertation. University of Dayton, Dayton OH,
 1999b.
- Myers, L. E., G. D. Miller, R. C. Eckardt, M. M. Fejer, R. L. Byer, and W. R. Bosenberg.
 "Quasi-phase-matched 1.064-um-pumped optical parametric oscillator in bulk
 periodically poled LiNbO₃," Optics Letters, 20: 52-54 (January 1995a).
- , R. C. Eckardt, M. M. Fejer, R. L. Byer, W. R. Bosenberg, and J. W. Pierce. "Quasi-
 phase-matched optical parametric oscillators in bulk periodically poled LiNbO₃,"
J. Opt. Soc. Am. B, 12: 2102-2115 (November 1995b).
- , M. L. Bortz, M. A. Arbore, R. C. Eckardt, M. M. Fejer, R. L. Byer, and W. R.
 Bosenberg. "Quasi-phases-matched optical parametric oscillators in periodically
 poled LiNbO₃," Optics and Photonics News: 30 (December 1995c).
- , R. C. Eckardt, M. M. Fejer, R. L. Byer, and W. R. Bosenberg. "Multigrating quasi-
 phase-matched optical parametric oscillator in periodically poled LiNbO₃," Optics
 Letters, 21: 591-593 (April 1996).
- Pollock, David H. The Infrared & Electro-Optical Systems Handbook (Vol. 7,
 Countermeasure Systems). Bellingham Washington: SPIE Optical Engineering
 Press, 1993.
- Rabin, Herbert and C. L. Tang. Quantum Electronics: A Treatise (Vol. 1, Nonlinear
 Optics, Part B). New York: Academic Press, 1975.
- Reid, D. T., Z. Penman, M. Ebrahimzadeh, W. Sibbett, H. Karlsson, and F. Laurell.
 "Broadly tunable infrared femtosecond optical parametric oscillator based on
 periodically poled RbTiOAsO₄," Optics Letters, 22: 1397-1399 (September 1997).
- Roh, Won B. Class lectures, OENG 660, Introduction to Nonlinear Optical Devices.
 Graduate School of Engineering, Air Force Institute of Technology, Wright-
 Patterson AFB OH, Winter Quarter 1999.

- , Class lectures, OENG 620, Laser Engineering. Graduate School of Engineering, Air Force Institute of Technology, Wright-Patterson AFB OH, Spring Quarter 1999.
- Ruff, J. A. and A. E. Siegman. "Single-pulse laser beam quality measurements using a CCD camera system," Applied Optics, 31: 4907-4909 (August 1992).
- Schepler, Kenneth L. "Trends in solid-state lasers," Optics and Photonics News: 39-41 (January 1997).
- , Mark J. Missey, Ned O'Brien, and Peter Powers. "Power and energy scaling for quasi-phases-matched OPOs," SPIE, 3793: 187-195 (July 1999).
- Schneider, K., P. Kramper, S. Schiller, and J. Mlynek. "Toward an optical synthesizer: a single frequency parametric oscillator using periodically poled LiNbO₃," Optics Letters, 22: 1293-1295 (September 1997).
- Schubert, Max, and Bernd Wilhelm. Nonlinear Optics and Quantum Electronics. New York: Wiley-Interscience, 1986.
- Seyrafi, Khalil and S. A. Hovanesian. Introduction to Electro-Optical Imaging and Tracking Systems. Boston MA: Artech House, 1993.
- Siegman, A. E. "Defining, measuring, and optimizing laser beam quality," SPIE, 1868: 2-11 (Jan 1993).
- Stolzenberger, Richard and Michael Scripsick. "Recent advancements in the periodic poling and characterization of RTA and its isomorphs," SPIE, 3610: 23-35 (January 1999).
- Suzaki and Atsushi Tachibana. "Measurement of the μm sized radius of Gaussian laser beam using the scanning knife-edge," Applied Optics, 14: 2809-2810 (December 1975).
- Vaidyanathan, M., R. C. Eckardt, Vince Dominic, L. E. Myers, and T. P. Grayson. "Cascaded optical parametric oscillations," Optics Express, 1: 49-53 (July 1997).
- Verdeyen, Joseph T. Laser Electronics (Third Edition). New Jersey: Prentice Hall, 1995.
- Yang, Steven T. and Stephan P. Velsko. "Frequency-agile kilohertz repetition-rate optical parametric oscillator based on periodically poled lithium niobate," Optics Letters, 24: 133-135 (February 1999).

Yariv, Amnon and Pochi Yeh. Optical Waves in Crystals. New York: John Wiley & Sons, 1984.

Zayhowski, John J. "Periodically poled lithium niobate optical parametric amplifiers pumped by high power passively Q-switched microchip lasers," Optics Letters, 22: 169-171 (February 1997).

Vita

Lieutenant Frank J. Glavic was born in Wickliffe, Ohio on 26 April 1968. After graduating from Wickliffe High School in 1986, he enlisted and began his Air Force career through Basic Military Training at Lackland AFB, Texas. Frank was assigned to the Air Force Technical Applications Center (AFTAC) and was selected for maintenance technician duty at the Detachment 452 Seismological Research Station, located in the Republic of Korea. Frank's additional AFTAC assignments included engineering at the Technical Operations Division and development and maintenance at the McClellan Central Laboratory Rare-Gas Analysis Lab; both units were located in Sacramento, California. He completed an Associate's Degree in Electronic Systems Technology through the Community College of the Air Force in 1990. After completion of his enlistment, Lt. Glavic was employed at Rockwell Automation in Cleveland, Ohio. While pursuing a bachelor's degree, he progressed from a Senior Control System Tester to a Development Engineer and Supervisor—designing Rockwell's high-performance, 5,000-horsepower motor drive. He completed his Bachelor's Degree in Electrical Engineering, Magna Cum Laude, from Cleveland State University in 1996 and applied for USAF Officer Training School. Lieutenant Glavic was commissioned on February 7, 1997, and was assigned to the 90th Space Wing, F. E. Warren AFB, Wyoming. He worked as a Technical Engineer on Peacekeeper and Minuteman III inter-continental ballistic missiles until entering the Air Force Institute of Technology graduate program in August 1998.

REPORT DOCUMENTATION PAGE			Form Approved OMB No. 0704-0188	
Public reporting burden for this collection of information is estimated to average 1 hour per response, including the time for reviewing instructions, searching existing data sources, gathering and maintaining the data needed, and completing and reviewing the collection of information. Send comments regarding this burden estimate or any other aspect of this collection of information, including suggestions for reducing this burden, to Washington Headquarters Services, Directorate for Information Operations and Reports, 1215 Jefferson Davis Highway, Suite 1204, Arlington, VA 22202-4302, and to the Office of Management and Budget, Paperwork Reduction Project (0704-0188), Washington, DC 20503.				
1. AGENCY USE ONLY (Leave blank)	2. REPORT DATE March 2000	3. REPORT TYPE AND DATES COVERED Master's Thesis		
4. TITLE AND SUBTITLE TUNABLE MID-IR OPTICAL PARAMETRIC OSCILLATOR USING PERIODICALLY POLED RUBIDIUM TITANYL ARSENATE		5. FUNDING NUMBERS		
6. AUTHOR(S) Frank J. Glavic, 1Lt, USAF				
7. PERFORMING ORGANIZATION NAME(S) AND ADDRESS(ES) Air Force Institute of Technology 2750 P Street WPAFB, OH 45433-7765		8. PERFORMING ORGANIZATION REPORT NUMBER AFIT/GEO/ENP/00M-2		
9. SPONSORING/MONITORING AGENCY NAME(S) AND ADDRESS(ES) Dr. Kenneth L. Schepler AFRL/SNJT 3109 P Street WPAFB, OH 45433-7765 Phone: 937-255-3804 x312		10. SPONSORING/MONITORING AGENCY REPORT NUMBER		
11. SUPPLEMENTARY NOTES Dr. Won B. Roh, AFIT/ENP				
12a. DISTRIBUTION AVAILABILITY STATEMENT Approved for public release; distribution unlimited.		12b. DISTRIBUTION CODE		
13. ABSTRACT (Maximum 200 words) <p>Tunable sources of coherent radiation are needed for a variety of military and commercial applications, including infrared countermeasures and atmospheric remote sensing. This research investigates a tunable mid-infrared coherent source using periodically-poled rubidium titanyl arsenate (PPRTA) as a quasi-phase matched (QPM) optical parametric oscillator (OPO). The advantages of PPRTA over periodically poled lithium niobate (PPLN) are presented.</p> <p>Quasi-phase matching and periodic poling theory are discussed, along with some important historical results and current developments. Experimental setups for determining threshold, conversion efficiency, pump depletion, and beam quality are presented along with experimental results. The research effort is focused on characterizing PPRTA through the generation of tunable midinfrared laser radiation in the 1.4 to 4.0 micron region.</p> <p>Results successfully demonstrate PPRTA conversion in the 1.5 um range with a 173 mJ oscillation threshold and a beam quality (M2) value of 9.0. Slope efficiency of PPRTA is shown to be 24%, compared to slope efficiency of 15% for PPLN in an identical system setup. The high slope efficiency, high pump conversion (~ 60%), absence of damage at pump levels in excess of 300 MW/cm², and large aperture scaling possibilities suggest that PPRTA is well suited for higher power applications.</p>				
14. SUBJECT TERMS Tunable Laser, Infrared, Quasi-Phase Match, QPM, Periodic-Poling, Optical Parametric Oscillator, OPO, Rubidium Titanyl Arsenate, RTA, Lithium Niobate, PPLN, Mid-IR			15. NUMBER OF PAGES 58	
			16. PRICE CODE	
17. SECURITY CLASSIFICATION OF REPORT Unclassified	18. SECURITY CLASSIFICATION OF THIS PAGE Unclassified	19. SECURITY CLASSIFICATION OF ABSTRACT Unclassified	20. LIMITATION OF ABSTRACT UL	